ELSEVIER

J. Non-Newtonian Fluid Mech. 125 (2005) 11–23

Journal of Non-Newtonian Fluid Mechanics

www.elsevier.com/locate/jnnfm

Impact dynamics of drops on thin films of viscoelastic wormlike micelle solutions

Joshua Lampe*, Robert DiLalla, Jason Grimaldi, Jonathan P. Rothstein

Department of Mechanical and Industrial Engineering, University of Massachusetts, Amherst, MA 01003, USA

Received 28 May 2004; received in revised form 4 August 2004; accepted 28 August 2004

Abstract

The impact dynamics of water drops on thin films of viscoelastic wormlike micelle solutions is experimentally studied using a high-speed digital video camera at frame rates up to 4000 frame/s. The composition and thickness of the thin film is modified to investigate the effect of fluid rheology on the evolution of crown growth, the formation of satellite droplets and the formation of the Worthington jet. The experiments are performed using a series of wormlike micelle solutions composed of a surfactant, cetyltrimethylammonium bromide (CTAB), and a salt, sodium salicylate (NaSal), in deionized water. The linear viscoelastic shear rheology of the wormlike micelle solutions is well described by a Maxwell model with a single relaxation time while the steady shear rheology is found to shear thin quite heavily. In transient homogeneous uniaxial extension, the wormlike micelle solutions demonstrate significant strain hardening. The size and velocity of the impacting drop is varied to study the relative importance of Weber, Ohnesorge, and Deborah numbers on the impact dynamics. The addition of elasticity to the thin film fluid is found to suppress the crown growth and the formation of satellite drops with the largest effects observed at small film thicknesses. A new form of the splashing threshold is postulated which accounts for the effects of viscoelasticity and collapses the satellite droplet data onto a single master curve dependent only on dimensionless film thickness and the underlying surface roughness. Additionally, a plateau is observed in the growth of the maximum height of the Worthington jet height with increasing impact velocity. It is postulated that the complex behavior of the Worthington jet growth is the result of a dissipative mechanism stemming from the scission of wormlike micelles.

Keywords: Drop impact; Wormlike micelle solutions; Surfactant solutions; Viscoelastic; Satellite drop; Worthington jet

1. Introduction

Complex fluids such as polymer melts and solutions, suspensions, and micelle solutions are encountered in a variety of industries and applications critical to modern day economies. Micelle solutions are currently being used extensively as rheological modifiers in consumer products such as paints, detergents, and pharmaceuticals where careful control of the fluid properties is required. In addition, micelle solutions have also become important in a wide range of applications including agrochemical spraying, inkjet printing, and enhanced oil recovery. A fundamental understanding of the behavior of these complex fluids in different flow regimes is therefore of critical importance [1–5].

Surfactants are surface-active molecules that consist of a hydrophilic head group and a hydrophobic tail. When dissolved in water the surfactants will diffuse to the interfaces, significantly reducing surface tension. As the concentration of the surfactant is increased and the interfaces become saturated, the surfactants can spontaneously self-assemble to form several different types of aggregates in the bulk fluid [6–8]. The morphologies of these aggregates can range in shape and size from spherical micelles, to wormlike micelles, to lamellae depending on surfactant, and counterion concentration. Under the proper conditions, the micelles, resembling slender rods, can entangle and impart viscoelasticity to the fluid [1]. The behavior of wormlike micelle solutions is sim-

* Corresponding author.
E-mail address: jprothstein@ecs.umass.edu (J. Lampe).

0377-0257/$ – see front matter © 2004 Elsevier B.V. All rights reserved.
doi:10.1016/j.jnnfm.2004.08.012

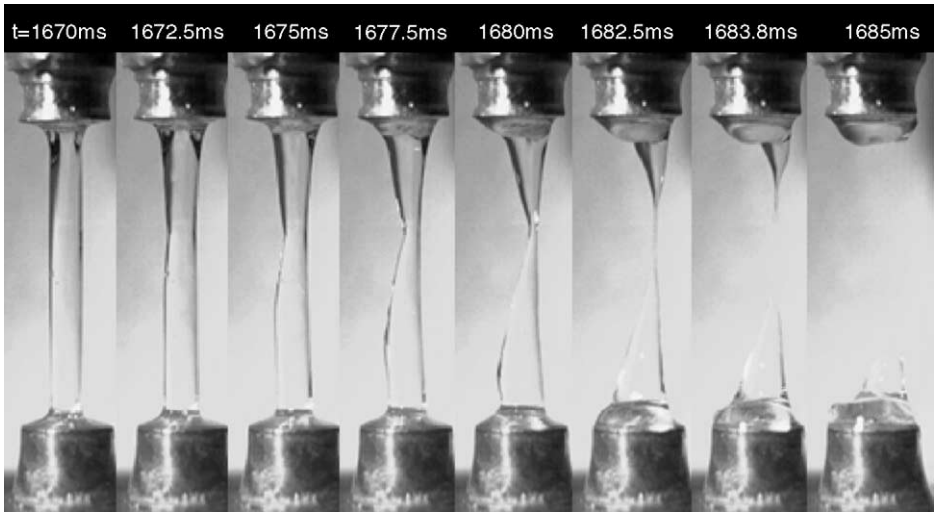

Fig. 1. Series of images showing the rupture of a filament of 0.05 M CTAB 0.05 M NaSal wormlike micelle solution in a transient uniaxial extensional flow at a Deborah number is $De = 8.8$. The filament achieves a final Hencky strain of $\varepsilon_f = 2.5$ before failure.

ilar to that of polymer solutions and melts. The primary difference being that unlike a covalently bonded polymer backbone, micelles are in a state of thermodynamic equilibrium with the solvent and are perpetually broken and reformed under Brownian fluctuations. This leads to a broad and dynamic distribution of micelle lengths, which can change under an imposed shear or extensional flow [9].

The break-up dynamics of droplets and jets of complex fluids such as micelle solutions are governed by the extensional viscosity and surface tension of these non-Newtonian fluids. The dynamical response of complex fluids in extension is quite different than in simple shear [10]. Whereas the shear viscosity of a typical micelle solution will heavily thin with increasing shear rate, the extensional viscosity can increase by several orders of magnitude with increasing strain [4,11]. This strain hardening has been found to stabilize jets and drops of viscoelastic fluids by resisting the extensionally dominated flow leading to break-up resulting from capillary stresses [12–14]. In order to understand and predict the impact dynamics of a droplet on wormlike micelle solution thin film, detailed knowledge of both the shear and extensional rheology is essential.

Prud'homme and Warr [15] were the first to perform a comprehensive study of the extensional rheology of wormlike micelle solutions using a Rheometrics RFX opposed jet device. At large extension rates, chain stretching within the oriented segments was observed to lead to strain-hardening in the extensional rheology. Rothstein [4] later used a filament stretching rheometer to study the transient extensional rheology of a series of cetyltrimethylammonium bromide (CTAB) and sodium salicylate (NaSal) solutions with similar results. Although polymer and wormlike micelle solutions exhibit similar behavior in strong extensional flows, wormlike micelle solutions can exhibit a wide array of complex flow behaviors not observed for polymer solutions [4,11]. For example, a filament or jet of polymer solution in an extensional flow tends to pinch off and fail through an elastocapillary, Rayleigh-type instability [14]. By comparison, the filament stretching experiments on a series of the wormlike micelle solutions performed by Rothstein [4] came to an abrupt end with the dramatic rupture of the fluid filament near its axial midplane. As can be seen from the series of high-speed images in Fig. 1, the filament failure is not the result of elastocapillary thinning, but instead, the filament exhibits an instability, which is unique to wormlike micelle solution and other self assembling systems [4]. A similar instability was also observed by Smolka and Belmonte [16] during the pinch-off of a pendant drop of several wormlike micelles solutions. Rothstein [4] hypothesized that this filament failure stems from the scission of wormlike micelles resulting in a dramatic breakdown of the micelle network structure en masse. This interpretation was supported by Prud'homme and Warr [15] who found that at a critical Deborah number, the extensional viscosity was observed to reach a maximum and decreases with further increases in Deborah number. They theorized and later showed through light scatter measurements that the observed reduction in the extensional viscosity at high extension rates was the result of a scission of the wormlike micelles in the strong extensional flow [15,17]. The response of micelle solutions in purely extensional flows has been found to lead to new and interesting instabilities in more complex flows such as the flow past a sphere falling through a wormlike micelle solution [11,18] and bubbles rising through wormlike micelles solutions [19,20] and could have a significant effect on droplet impact dynamics and satellite droplet formation.

The initial spreading and deformation of a droplet impacting a liquid or solid surface is dominated by the inertial and viscous forces [21]. In Fig. 2, a sequence of images is shown for a water droplet impacting a thin film of water. Upon impact, an enormous pressure impulse similar to water hammer is created within the droplet and the thin film. As seen in Fig. 2b, the droplet spreads outward forming a

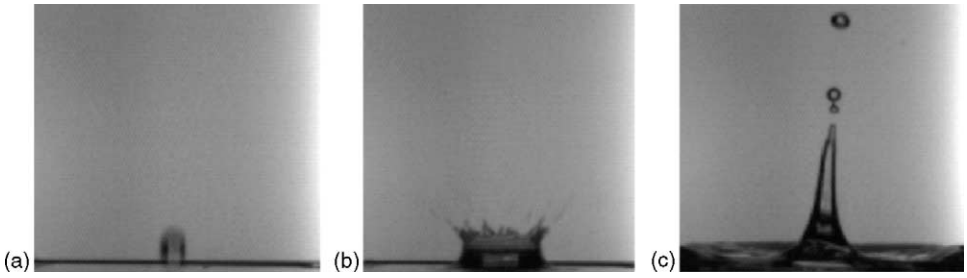

Fig. 2. High-speed digital video images (2000 frame/s) of the impact of a water drop (D_0 = 4.6 mm, u = 3.6 m/s) on a thin film of water (t_f = 5.1 mm). The images show (a) the droplet just prior to impact; (b) the crown and satellite droplet formation; (c) the formation of a Worthington jet.

crown as it is slowed by viscous forces and surface tension. Splashing, which is defined by the formation of secondary droplets, is observed for impacting droplets with sufficient initial energy that jetting becomes possible from the crown [22]. The crown eventually collapses and, as seen in Fig. 2a and c, Worthington jet is formed as the fluid rushes back into the crater left by the impacting drop. It has been shown by Stow and Hatfield [23] that the splashing threshold, K_L, can be expressed in terms of an Ohnesorge number and a Weber number.

$$K_L = Oh^{-0.37}\, We = \left(\frac{\mu}{\sqrt{\rho\sigma 2R_0}}\right)^{-0.37}\left(\frac{\rho U^2 2R_0}{\sigma}\right), \quad (1)$$

where μ is the Newtonian viscosity, ρ the density, σ the surface tension, R_0 the initial droplet radius, and U is the droplet impact velocity. The droplet impact dynamics have been studied for Newtonian fluids on dry surfaces with various surface roughness, R_{ND}, and on Newtonian films with various film thicknesses, t_f [21–25]. For a Newtonian fluid, the threshold for splashing, $K_L = f(\delta, R_{ND})$, has been found to be a function of the dimensionless film thickness, $\delta = t_f/D_0$, and the surface roughness [24].

A series of experiments have also been performed studying the effect of dynamic surface tension and elasticity on the impact of dilute polymer solutions and surfactant solutions on dry surfaces [26–29]. These studies were motivated by the need to suppress the secondary drop formation and drop rebounding during agrochemical spraying, spray coating or inkjet printing. These studies demonstrated that the addition of a small amount of polymer solution or wormlike micelles dramatically increases the threshold for splashing and drop rebounding. These studies found that the drop impact dynamics are a strong function of Deborah number, $De = \lambda\dot{\gamma}$, which describes the relative importance of elastic and viscous stresses. Here, λ is the relaxation time of the fluid and $\dot{\gamma}$ is the shear rate. A series of experiments by Cheny and Walters [30] investigated the effects of elasticity on the Worthington jet height resulting from the impact of a solid sphere with a deep reservoir of dilute polymer solution. They showed that the large extensional viscosities of these polymer solutions resulted in a significant reduction in the maximum height reached by the Worthington jet [30]. Cheny and Walters [30] also performed the only studies to date to investigate the impact dynamics of liquid drops on reservoirs of non-Newtonian fluids although the results of their experiments were presented as a series of qualitative pictures and not fully quantified [31].

There are currently no experimental or numerical data showing how elasticity and shear thinning affect the impact dynamics of droplets on thin films or deep reservoirs of surfactant solutions. In this manuscript, we will quantify the functional dependence of the Worthington jet height, crown formation, splashing threshold and the satellite drops resulting from the impact of a drop on a thin film of wormlike micelle solution on the film thickness, Deborah number, Weber, and Ohnesorge number.

The outline of this paper is as follows. In Section 2, we briefly describe the experimental setup, the implementation of several measurement techniques and the shear and extensional rheology of the wormlike micelle solution used. In Section 3, we discuss the experimental results and in Section 4 we conclude.

2. Experimental

2.1. Flow geometry and experimental setup

A schematic diagram of the flow geometry and experimental setup is shown in Fig. 3. A high-speed, high-resolution digital video camera (Kodak Motion Corder Sr) was used to observe the drop impact dynamics and follow the evolution of crown growth, the size and number of satellite droplets, and the height of the Worthington jet. For each surfactant solution, the size, velocity and composition of the impacting droplet was varied to study the relative importance of Weber number, Ohnesorge number and thin film thickness on the impact dynamics.

A series of 5 cm square acrylic and glass dishes were fabricated and used to contain the desired thin films. The depth of the fluid was precisely determined for each experiment by measuring the thickness of thin film resulting from the addition of a known volume of fluid. A fine, 1 cm long stylus was inserted into the fluid and imaged using the digital video camera. The images were processed using a MATLAB^{TM} routine, which calculated the thickness of the thin film from the difference between a calibration image of the full stylus

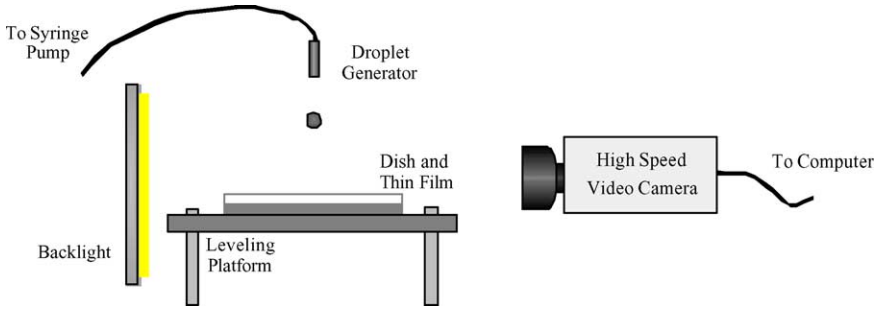

Fig. 3. Schematic diagram of the experimental setup.

and the length of the stylus visible after immersion in the thin film.

Droplets were generated with a syringe pump (KD Scientific 100) used to expel a known volume of fluid out of the end of a length of flexible plastic tubing. The size of the droplets generated was determined both by determining the mass (Mettler AC100) of a series of drops and by comparing the image of a falling drop to an optical scale. The size of the drops generated was modified by changing the diameter of the tubing resulting in drops with diameters of $D_0 = 3.59$ mm and 4.56 mm.

The impact velocity of the drop and thus the Weber number were modified by changing the release point of the droplet. The velocity of the droplet upon impact was not always measured explicitly for each experiment, instead it can be shown that the velocity of the falling drop can be fit by the following expression [32]

$$U = \sqrt{\frac{9.81}{A}(1 - e^{-2Ah})}, \tag{2}$$

where h is the release height of the drop and the coefficient A is a given by

$$A = \frac{3}{8}\frac{C_f \rho_{air}}{\rho_{drop} R_0}, \tag{3}$$

where ρ_{air} is the density of the air, ρ_{drop} the density of the drop, and C_f is the empirically fitted drag coefficient on the drop. To determine the drag coefficient, a series of experiments were performed to determine the velocity of a falling droplet as a function of its release point. The position of the center of mass of the drop was determined in successive high-speed video images using a MATLAB^{TM} routine. The velocity of the drop was then determined by dividing the distance the drop fell by the time lapse. Using a least squares fit of Eq. (2) through the data, a drag coefficient of $C_f = 0.63$ was found. This value is in good agreement with previously experimental results [26,32].

2.2. Test fluids

The test fluids are a series of equimolar wormlike micelle solutions of a surfactant, CTAB (Fisher Scientific), and a salt, NaSal (Fisher Scientific), in deionized water. The concentration of the surfactant and the salt in solution were varied from $10 \leq$ mM ≤ 25. Each of these solutions is well above the critical micelle concentration, which for CTAB in pure water is CMC = 0.9 mM and can be reduced by the addition of salt [6]. At these concentrations, the wormlike micelle solutions are concentrated and entangled with significant number of entanglement points per chain [6]. The solutions were prepared and allowed to equilibrate at room temperature for several days before experiments were performed.

The equilibrium surface tension for each of the wormlike micelle solutions tested was assumed to be consistent with the value of $\sigma = 0.036$ N/m reported in the literature for CTAB/NaSal solutions above the CMC [27]. However, because of the relatively short timescales associated with the droplet impact experiments, Cooper-White et al. [27] showed that it is the dynamic and not the equilibrium surface tension which is the relevant quantity. As the thin film and impacting droplet are deformed and new surface is generated, CTAB molecules diffuse from the bulk and populate the new surface. The timescale for repopulating the surface can be long in comparison to the timescales associated with generating new surface. Using a maximum bubble pressure tensiometer, Cooper-White et al. [27] measured the dynamic surface tension of a series of CTAB/NaSal solutions. Above the CMC, the dynamic surface tension behavior was found to be independent of surfactant concentration. At short times, up to about 15 ms after the creation of a new surface, the dynamic surface tension equals that of water ($\sigma = 0.070$ N/m). As time progresses, the surface tension decays, eventually approaching an equilibrium value of $\sigma = 0.036$ N/m after about 1000 ms [27]. As the timescale for the impact dynamics of interest occur over very short timescales, the equilibrium surface tension of water will be used to calculate the necessary dimensionless parameters.

2.3. Shear rheology

The steady and dynamic shear rheology of the test fluid was characterized using a TA cone-and-plate controlled stress rheometer (Model AR2000) with a 6 cm diameter and 1° truncated cone. The micelle solutions were loaded and allowed to equilibrate at $T = 25$°C for several minutes. The samples were not presheared. The results of the linear viscoelastic-

Table 1
Parameters characterizing the shear rheology of the CTAB and NaSal wormlike micelle solutions

CTAB [M]	NaSal [M]	Viscosity, η_0 [Pa s]	Modulus, G_N^0 [Pa]	Relaxation time, λ [s]
0.01	0.01	5.0	0.28	18
0.0175	0.0175	41	1.2	35
0.025	0.025	68	2.5	27

ity measurements are shown in Fig. 4. The storage modulus, G', and loss modulus, G'', of the wormlike micelle solutions with concentrations of 10 mM, 17.5 mM, and 25 mM CTAB/NaSal are plotted in Fig. 4 as a function of angular frequency, ω. Cates [1] proposed that, in the fast breaking-limit, $\lambda_d \gg \lambda_{break}$, the relaxation time, $\lambda = (\lambda_{break}\lambda_d)^{1/2}$, is a function of the repetition or disentanglement time of the micelle in solution, λ_d, and the characteristic timescale for break-up and reformation of a wormlike micelle, λ_{break} [1,2]. In Table 1, the zero-shear-rate viscosity η_0, relaxation time λ and elastic plateau modulus $G_N^0 = \eta_0/\lambda$, determined by fitting a single-mode Maxwell model to the low frequency data are listed for each viscoelastic surfactant solution. The linear viscoelastic data and the predictions of the Maxwell models are in good agreement for all of the wormlike micelle solutions tested over much of the dynamic range. However, deviations are observed at large angular frequencies corresponding to the Rouse-like behavior of the micelle between entanglement points [33]. This deviation, which becomes more pronounced as the concentration of surfactant and salt and therefore the number of entanglements per chain are reduced, is consistent with observations in the literature [34,35]. Using the models developed by Cates et al. [36,37] the Rouse relaxation time, λ_{Rouse}, was approximated from the upturn in the G'' data. The Rouse relaxation time was then used to determine the characteristic break-up and reformation time of the micelle [37]. For the three solutions presented in Fig. 4, 200 ms < λ_{break} < 350 ms. In the fast breaking limit, $\lambda_{break} \ll \lambda_{Rouse} \ll \lambda$, however, as we will show in Section 3, all three of these timescales are long when compared to the dynamics of droplet impact.

In Fig. 5, the steady shear viscosity, η, is plotted as a function of shear rate, $\dot{\gamma}$ for the three fluids used. At small shear rates the viscosity plateaus [38]. As the shear rate is increased, the fluids begin to heavily shear thin, the shear stress plateaus and the viscosity dependence on shear rate approaches a slope of $\eta \propto \dot{\gamma}^{-1}$. Superimposed over the experimental data in Fig. 5 are the predictions of the Giesekus model [38] with the non-linear parameter $\alpha = 0.25$ for all the micelle solutions tested. The Giesekus model is a good fit to the data over the entire range of shear rates.

2.4. Extensional rheology

A filament stretching rheometer capable of imposing a homogeneous uniaxial extension on a fluid filament placed between its two endplates was used to make simultaneously measurements of the evolution of the force, the midpoint radius and the flow induced birefringence of the fluid filament. A complete description of the design and operating space of the filament stretching rheometer used in these experiments can be found in Rothstein and McKinley [39,40].

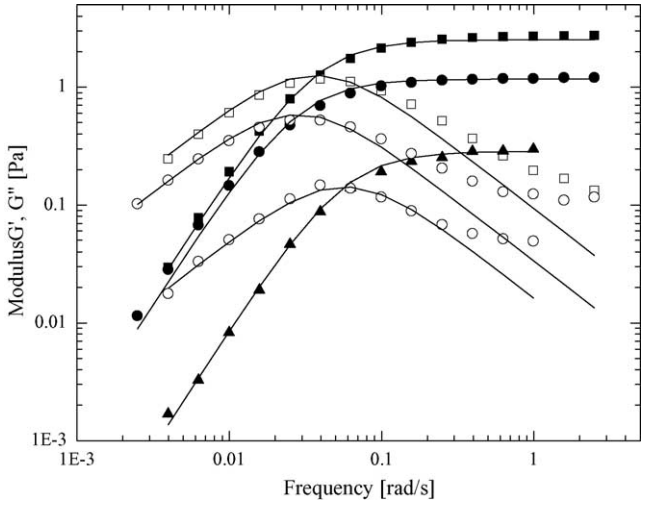

Fig. 4. Linear viscoelastic shear rheology of the wormlike micelle solutions used. The filled symbols denote the storage modulus G' while the open symbols denote the loss modulus G''. The data include: (▲) 10 mM CTAB/NaSal; (●) 17.5 mM CTAB/NaSal; (■) 25 mM CTAB/NaSal; (—) the fit from a single mode Maxwell model.

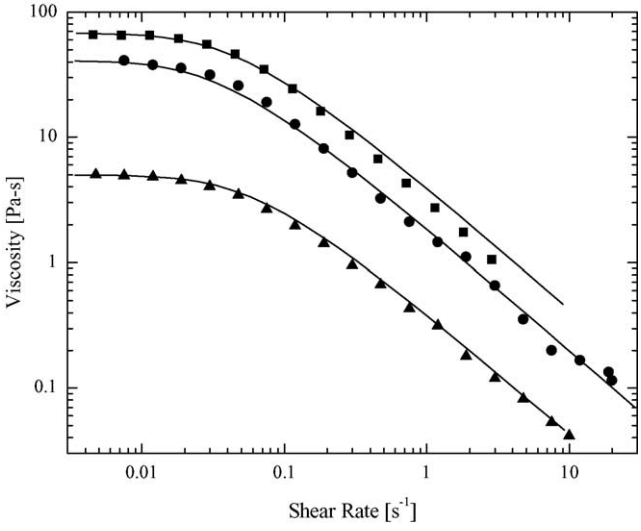

Fig. 5. Steady shear rheology of the wormlike micelle solutions used. The experimental data include aqueous solutions of (▲) 10 mM CTAB/NaSal; (●) 17.5 mM CTAB/NaSal; (■) 25 mM CTAB/NaSal. The experimental data is compared to the predictions of: (—) the Giesekus model.

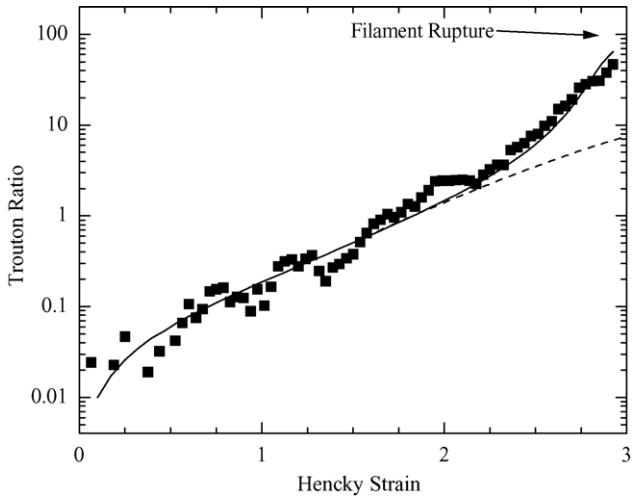

Fig. 6. Transient homogeneous uniaxial extensional rheology of 25 mM CTAB 25 mM NaSal wormlike micelle solution at a Deborah number of $De = 8.8$. The experimental data shows the growth of the tensile stress (■) as a function of Hencky strain. The data is compared to the predictions of: a FENE-PM model (—) and a Giesekus model (- - -).

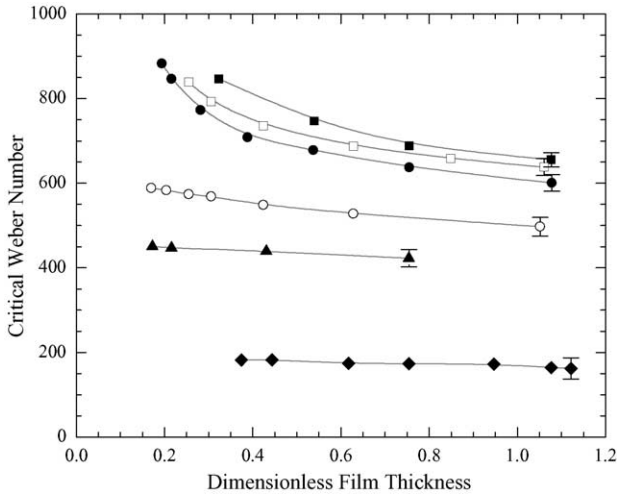

Fig. 7. Critical Weber number for the appearance of satellite drops as a function of dimensionless film thickness. The filled symbols represent impacting water drops of diameter $D_0 = 3.59$ mm while the open symbols represent impacting water drops of diameter $D_0 = 4.56$ mm. The data include aqueous solutions of (▲) 10 mM CTAB/NaSal; (●) 17.5 mM CTAB/NaSal; (■) 25 mM CTAB/NaSal; (♦) water. The lines through the data are not a quantitative fit, but are simply to guide the eye.

In Fig. 6, the Trouton ratio, $Tr = \eta_E^+/\eta_0$, which is a non-dimensionalized transient extensional viscosity, η_E^+, is plotted as a function of accumulated Hencky strain, $\varepsilon = \dot{\varepsilon}t$ for the 25 mM CTAB/NaSal wormlike micelle solution at a Deborah number of $De = \lambda\dot{\varepsilon} = 49$. At a Hencky strain of $\varepsilon = 2.9$, a dramatic rupture of the fluid filament occurs near its axial midplane, see Fig. 1. The wormlike micelle solution demonstrates considerable strain hardening and appears to approach an equilibrium value of the Trouton ratio around $Tr \approx 50$. No significant contribution to the Trouton ratio from the aqueous solvent is observed. The growth of the elastic tensile stress is well predicted by a multimode FENE-P model [4,41], however, the Giesekus model, which did an excellent job predicting the shear rheology, significantly underpredicts the growth in the elastic tensile stress. For a more detailed discussion of the constitutive model fits to the extensional and shear rheology of wormlike micelle the reader is directed to the recent literature [4,11].

3. Results and discussion

3.1. Impact experiments

The impact dynamics of water droplets were studied for a series of thin films of both water and viscoelastic entangled wormlike micelle solutions composed of equimolar CTAB and NaSal solutions in water having molarities between 10 mM and 25 mM. In Fig. 7, the critical Weber number for the formation of satellite droplets from the crown is presented as a function of dimensionless thin film thickness. To determine the critical Weber number, drops were released from successively larger heights until satellite droplets were observed. A new thin film was generated and allowed to equilibrate for at least 20 min before each impact experiment. The data in Fig. 7 represent the average critical Weber number determined from a series of experiments. The repeatability of these experiments was relatively good, however, as observed by Cossali et al. [24] and others, at nominally identical experimental conditions very close to the critical Weber number the impact can either result in the production of satellite drops or not making it difficult to identify an exact critical Weber number. The uncertainty in the splashing threshold is represented by the characteristic error bars superimposed over the data in Fig. 7. The dependence of the critical Weber number on the dimensionless thin film thickness of the water is weak, decaying slowly as the depth of the water is increased. Both the trend and the magnitude of the critical Weber number for the impact on a thin film of water are in good agreement with the experimental results in the literature [24].

The impact dynamics of water droplets on thin films of viscoelastic micelle solutions are quite different from those of water and other Newtonian fluids. At large film thicknesses, $\delta > 1$, the critical Weber number for the formation of satellite drops is not a strong function of film thickness, decreasing slowly with increasing dimensionless film thickness for all the wormlike micelle solutions tested. For all the wormlike micelle solutions tested, the critical Weber number was found to be significantly larger than that of water. In addition, at a given dimensionless film thickness, the critical Weber number was found to increase with increasing CTAB concentration and decreasing drop size. These trends can be partially explained by the changing viscosity of the thin film fluids. As shown in Eq. (1), the threshold for satellite droplet formation even for a Newtonian film is a weak function of Ohnesorge number and thus the observed critical Weber number will in-

crease with the viscosity of the thin film. In the low shear rate limit, the viscosity of each of the micelle solutions is significantly larger than water and increases with increasing CTAB concentration. However, the shear viscosity of the micelle solutions thins quite heavily with increasing shear rate making it necessary to use the shear rate dependent viscosity $\eta(\dot{\gamma})$ when evaluating the Ohnesorge number and the splashing threshold, K_L.

As the dimensionless film thickness is reduced, a nonlinear increase in the critical Weber number for satellite drop formation was observed for some of the micelle solutions. The observed dependence of the critical Weber number on the dimensionless film thickness for these non-Newtonian wormlike micelle solutions is qualitatively different than the droplet impact dynamics on thin films of water or other Newtonian fluids [23]. The onset of the upturn in the critical Weber number was found to move to larger dimensionless film thickness with increasing CTAB concentration and decreasing drop diameter. For thin films of the 25 mM CTAB solutions and a drop diameter of $D_0 = 3.59$ mm, no satellite droplets were observed for any of the experimentally obtainable Weber numbers below a critical dimensionless film thickness of approximately $\delta \approx 0.32$.

As seen in Fig. 2b, the kinetic energy of the impacting droplet causes the thin film to spread outward forming a crown as it is slowed by viscous stresses, surface tension and elastic stresses for the case of a viscoelastic fluid. If the impacting droplet has sufficient initial energy, the crown will bifurcate into a series of jets, which can eject satellite drops as they pinch off as a result of a Rayleigh instability [42]. The final break-up dynamics of the jets is an extensionally dominated flow driven by surface tension and resisted by the extensional viscosity of the fluid [43]. Although the shear viscosity of these micelle solutions thins heavily and approaches the viscosity of water at the shear rates produced by the droplet impact, the extensional viscosity increases dramatically, $Tr \gg 3$, as the strain and thus the micelle deformation is increased. This strain hardening of the extensional viscosity has been found to stabilize jet break-up of viscoelastic fluids [12–14,44] and one would certainly expect to observe similar stabilization here.

For 'strong' flows where $De > 0.5$, viscoelastic effects will become significant [38]. The characteristic shear rate of the droplet impact can be estimated as the impact velocity of the droplet divided by thickness of the thin film, $\dot{\gamma} = U/t_f$. The impact velocity of the droplet impact can be rewritten as:

$$U = \left(\frac{\sigma\, We}{\rho D_0}\right)^{1/2}. \tag{4}$$

By re-expressing the Deborah number as a function of Weber number,

$$De = \frac{\lambda U}{t_f} = \frac{\lambda}{t_f}\left(\frac{\sigma\, We}{\rho D_0}\right)^{1/2} = \frac{\lambda}{{t_f}^{3/2}}\left(\frac{\sigma\, We\, \delta}{\rho}\right)^{1/2}, \tag{5}$$

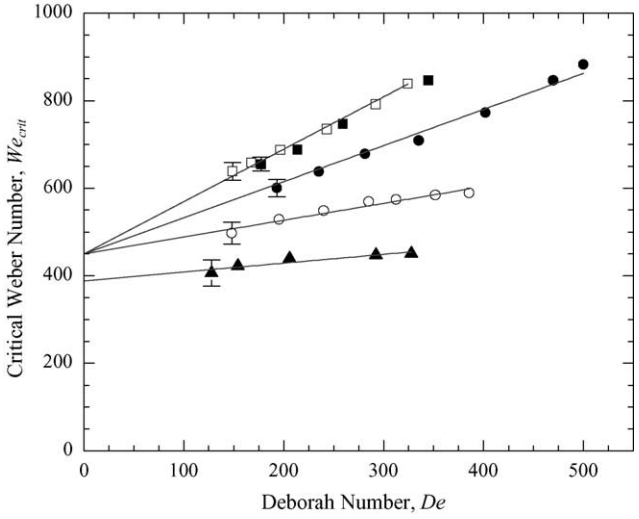

Fig. 8. Critical Weber number for the formation of satellite drops as a function of Deborah number. The filled symbols represent impacting water drops of diameter $D_0 = 3.59$ mm while the open symbols represent impacting water drops of diameter $D_0 = 4.56$ mm. The data include aqueous solutions of (▲) 10 mM CTAB/NaSal; (●) 17.5 mM CTAB/NaSal; (■) 25 mM CTAB/NaSal. The solid line represents a linear fit to the data.

it is possible to quantify the influence of elasticity on the form of the critical Weber number in Fig. 7. The relaxation time in Eq. (5) is evaluated as a function of shear rate, $\lambda(\dot{\gamma})$, using the Giesekus model fit the shear rheology described in Fig. 5. For a droplet impact experiment at a given Weber number, the Deborah number will increase linearly as the film thickness is decreased. Thus, if both the Weber number and dimensionless film thickness are fixed, the Deborah number will increase as the diameter of the impacting droplet is decreased and the effects of elasticity will be observed at progressively larger dimensionless film thicknesses.

If the critical Weber number is now plotted as a function of Deborah number, as in Fig. 8, the critical Weber number for satellite droplet formation is found to be linearly proportional to the Deborah number, $We_{crit} \propto De$. Substituting this result back into Eq. (5) it can be shown that

$$\delta \propto We_{crit}^{1/2}(We_{crit} - We_{\infty})^{-1}, \tag{6}$$

where We_∞ is the critical Weber number measured for the impact of a drop on an infinite reservoir of the surfactant solution or in other words, the Deborah number going to zero $De \to 0$. In the limit that $We_{crit} \gg We_\infty$, the critical Weber number scales as $We_{crit} \propto \delta^{-2}$, and thus the critical Weber number will approach infinity, $We_{crit} \to \infty$, as the dimensionless film thickness approaches zero, $\delta \to 0$, and the impact Deborah number approaches infinity, $De \to \infty$. The upturn in the critical Weber number and the suppression of the creation of satellite drops from the crown observed in Fig. 7 is thus a direct result of the increasing elasticity of the thin film, which is considerable at these large Deborah numbers.

This analysis suggests a new form of the splashing threshold for viscoelastic thin films

$$K_{\mathrm{L,VE}} = \frac{Oh^{-0.37}\,We}{De} = \left(\frac{\eta}{\sqrt{\rho\sigma 2R_0}}\right)^{-0.37}\left(\frac{\rho U^2 2R_0}{\sigma}\right)\left(\frac{t_\mathrm{f}}{\lambda U}\right). \quad (7)$$

In this equation, the viscosity, $\eta(\dot{\gamma})$, and relaxation time, $\lambda(\dot{\gamma})$, of the fluid are evaluated at the shear rate of impact using the Giesekus model fit to the steady shear data in Fig. 5. If the proposed scaling of Eq. (7) is correct, the experimental data should collapse onto a single master curve dependent only on the dimensionless film thickness. The splashing threshold is plotted as a function of dimensionless film thickness in Fig. 9 for all of the experiments presented in Fig. 7. The error bars incorporate both the error associated with the determination of the critical Weber number and the fit of the Giesekus model to the shear rheology. The data for a fixed CTAB/NaSal concentration but different drop diameters do indeed collapse onto a single master curve, thereby eliminating the effects of drop size observed in Fig. 7. However, the agreement of the data across all the CTAB/NaSal solutions is not as good. The data do appear to superimpose within experimental error onto a single curve at dimensionless thicknesses greater than $\delta > 0.5$ and asymptotically approach a splashing threshold of $K_{\mathrm{L,VE}} \approx 21$ for $\delta > 1$. However, the limitations of our scaling analysis become clear at dimensionless film thickness below $\delta < 0.5$.

There are several possible explanations for the observed deviation in the splashing threshold data. As the film thickness is reduced, the Weber numbers and therefore the shear rates required to produce satellite droplets increase beyond the range of the rheological data available in Fig. 5. At these very large shear rates, the accuracy of the Giesekus model predictions may be diminished. Additionally, the bifurcation of the crown into jets and their subsequent break-up into satellite droplets is a strong extensional flow and thus the extensional rheology and not just the shear rheology must be considered when developing a splashing threshold. A complete analysis would require knowledge about the extension rate and accumulated strain in the crown; whether the mode of failure of the jet is elastocapillary or a rupture event similar to that seen in Fig. 1; and even whether the droplet impact has induced new structure or a breakdown of the entangled micelle network. Unfortunately, such an analysis is difficult to develop in a simple scaling argument for the splashing threshold and would require detailed numerical simulations if one is to begin to understand in detail the influence of all these factors on the formation of satellite drops.

Crooks and Boger [26] studied the splashing threshold for a series of viscoelastic polyethylene oxide solution droplets impacting on dry surfaces. They found that the splashing threshold for viscoelastic fluids, $K_{\mathrm{L,VE}}$, could be related to the splashing threshold of Newtonian fluids, K_L, by considering the relaxation time of the fluid. Crooks and Boger [26] found that $K_{\mathrm{L,VE}} = K_\mathrm{L}/(1 - 1.07\,\lambda^{0.22})$ which is different from the scaling we arrived at in Eq. (7). The application of the scaling of Crooks and Boger to our data does not collapse it onto a single master curve even if we focus on a single drop size. However, this is not altogether surprising considering the many differences between our experiments and those of Crooks and Boger.

In Fig. 10, the maximum Worthington jet height is measured as a function of Weber number for the 10 mM CTAB/NaSal micelle solution for a series of dimensionless

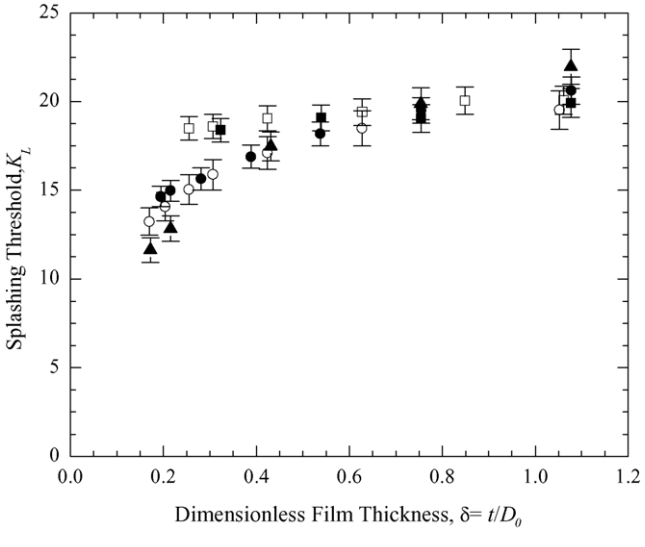

Fig. 9. Splashing threshold as a function of dimensionless film thickness. The filled symbols represent impacting water drops of diameter $D_0 = 3.59$ mm while the open symbols represent impacting water drops of diameter $D_0 = 4.56$ mm. The data include aqueous solutions of (▲) 10 mM CTAB/NaSal; (●) 17.5 mM CTAB/NaSal; (■) 25 mM CTAB/NaSal.

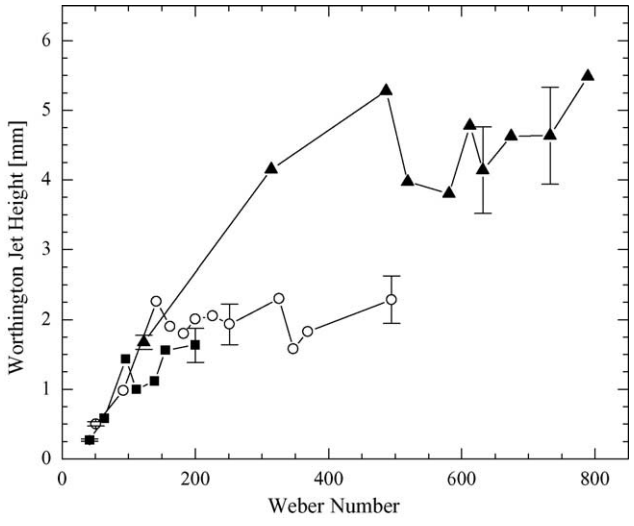

Fig. 10. Maximum Worthington jet height as a function of Weber number for the impact of a water drop of diameter $D_0 = 3.59$ mm on a thin film of a 10 mM CTAB/NaSal solution in water. The data include dimensionless film thickness of (▲) $\delta = 0.62$; (◯) $\delta = 0.55$; (■) $\delta = 0.5$.

film thicknesses. Each data point in Fig. 10 represents the average of three or more independent experimental measurements. As the Weber number is increased, the maximum height of the Worthington jet is initially observed to grow, but, at a critical Weber number, the jet height appears to approach and oscillate around a plateau. This complex behavior of the Worthington jet is qualitatively different from the monotonic growth observed for Newtonian fluids [31] and it has not previously been reported even for experiments with viscoelastic polymer solutions. To determine whether the scatter in the high Weber number data is significant or within the experimental error of the measurements, a series of 15 independent experiments were performed at several experimental conditions. The standard deviation of these experiments is represented in Fig. 10 by error bars superimposed over the data. The statistical analysis resulted in standard deviations between 3% and 5% at low Weber numbers during the growth of the Worthington jet and 15–18% at larger Weber numbers within the plateau. This suggests that the oscillations observed in the data may not be significant because the measurements the Worthington jet heights within the plateau region are indistinguishable from each other within experimental error.

As can be seen from Fig. 10, the qualitative behavior of the Worthington jet height growth is not affected by changing the dimensionless thin film thickness, however, the onset of the non-monotonic behavior occurs at lower Weber numbers as the film thickness is reduced and the Deborah number is increased. In all cases, the Worthington jet remains coherent and does not eject a secondary droplet and, in addition, the onset of the plateau in the Worthington jet height occurs well below the critical Weber number for the formation of satellite drops from the crown.

The dynamics of forming the Worthington jet results in a strong extensional flow within the jet. This extensional flow deforms and aligns the wormlike micelles within the jet as the fluid is stretched. As the Worthington jet grows and the accumulated strain increases, one would expect the extensional viscosity of the wormlike micelle solutions to strain harden perhaps resulting in the observed plateau of the Worthington jet height with increased Weber number. To analyze the extensional stresses in the Worthington jet, the extension rate of the flow within the Worthington jet was estimated by tracking the height of the jet, $h(t)$, as a function of time

$$\dot{\varepsilon}_{\text{jet}}(t) = \frac{1}{(t_{\text{f}} + h(t))} \frac{\mathrm{d}h(t)}{\mathrm{d}t}. \tag{8}$$

By fitting the height of the Worthington jet as a function of time to a third order polynomial, the extension rates were then calculated from Eq. (8). The extension rates were found to initially begin at no more than $\dot{\varepsilon} \approx 1000\,\text{s}^{-1}$ and to decay very quickly to zero after approximately 15 ms. To determine the total Hencky strain accumulated in the jet, the time dependent extension rate was integrated with respect to time from the onset of the jet formation to the time the jet reached its maximum height [39]

$$\varepsilon_{\text{jet}} = \int_0^t \dot{\varepsilon}_{\text{jet}}(t)\,\mathrm{d}t. \tag{9}$$

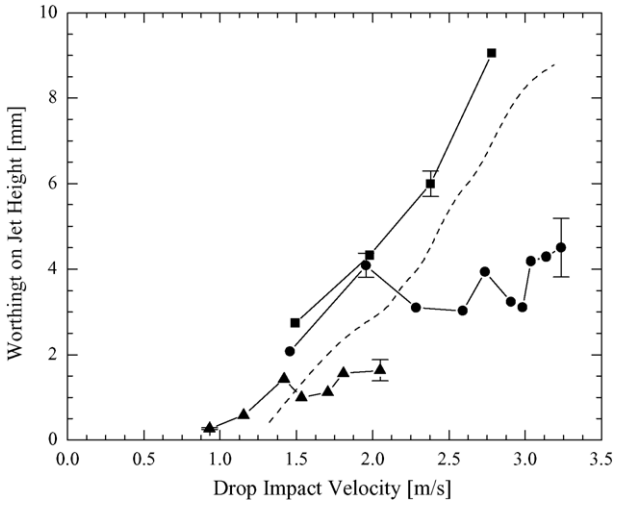

Fig. 11. Maximum Worthington jet height as a function of impact velocity a water drop of diameter $D_0 = 3.59$ mm on a thin film of dimensionless thickness $\delta = 0.5$. The experimental data include a series of aqueous wormlike micelle solutions: (▲) 25 mM CTAB/NaSal; (●) 17.5 mM CTAB/NaSal; (■) 10 mM CTAB/NaSal; (- - -) water.

In all cases, the resulting Deborah number was initially large enough to result in a coil-stretch transition and strain hardening of the wormlike micelle solutions, however, the total accumulated Hencky strain was in all cases found to be less than $\varepsilon < 1$. Because the Worthington jets do not attain significant heights, even in the presence of such a strong extensional flow, calculations using a multimode FENE-P model show that the extensional viscosity of the micelle solutions does not strain harden enough to significantly retard the development of the Worthington jet. If the Weber number is increased beyond the extent of the data in Fig. 10, the Worthington jets will break-up and eject satellite drops through a surface tension driven Rayleigh instability as shown in Fig. 2c. If significant strain hardening had occurred, one would expect to see a break-up of the Worthington jet similar to the filament rupture observed in Fig. 1. Of course this analysis assumes that the composition of the Worthington jet is that of the thin film. In actuality, the Worthington jet could be composed entirely of the water from the impacting drop or a much reduced concentration resulting from the mixing of the impacting drop with the thin film. In either case, the extension viscosity of the fluid within the jet will be further reduced from the extensional viscosity of the thin film. Thus, the plateau in the Worthington jet height is most likely not the result of strain hardening of the extensional viscosity. To study this phenomenon further, the growth of the Worthington jet height was studied as a function of surfactant concentration.

In Fig. 11, the maximum Worthington jet height as a function of drop impact velocity is shown for the impact

of a water droplet of diameter $D_0 = 3.59$ mm on thin films, $\delta = 0.5$, of a series of wormlike micelle solutions. Both the 10 mM CTAB/NaSal and 17.5 mM CTAB/NaSal solutions demonstrate the bounded behavior observed in Fig. 10. For this film thickness, the experimental measurements of the Worthington jet height of the 25 mM CTAB/NaSal solution were limited by the pinch-off and the subsequent release of a secondary droplet from the Worthington jet. The critical Weber number for the formation of secondary droplets from the Worthington jet was found to increase as the film thickness was reduced. At lower film thicknesses, by forestalling the onset of jet pinch-off, it was possible to observe the non-monotonic behavior of the Worthington jet height in the 25 mM CTAB/NaSal solutions as well. However, at the film thicknesses where the plateau was observed for the 25 mM CTAB/NaSal solutions, the Worthington jet produced by the 10 mM CTAB/NaSal solution was not large enough to produce a useful comparison between the different wormlike micelle solutions. Thus, a thickness of $\delta = 0.5$ was chosen for the presentation in Fig. 11. Within experimental error, the micelle solutions all appear to follow the same general trend in jet height growth as a function of impact velocity, however, the onset of the plateau in the Worthington jet height was found to move to lower impact velocities and Weber numbers as the concentration of the surfactant is reduced.

Although the Worthington jet height plateaus, the droplet impact dynamics do continue to change. In Fig. 12, a series of high speed images are shown to illustrate the evolution in the impact dynamics on a thin film of 17.5 mM CTAB/NaSal with dimensionless thickness $\delta = 0.5$ as the droplet impact velocity is increased from $U = 1.9$–3.2 m/s. These images correspond to points at the onset and the high end of the plateau shown in Fig. 11. Comparing the form of the Worthington jet between the two impact events, one observes that although the two jets are roughly equal in height, the jet in Fig. 12i, is much narrower than the jet in Fig. 12d, and becomes more blunt as it collapses. In addition, the crown that forms as a result of the larger impact velocity is taller, has a slightly larger diameter and has bifurcated into a series of fingers around its rim. The growth in the crown height and diameter was

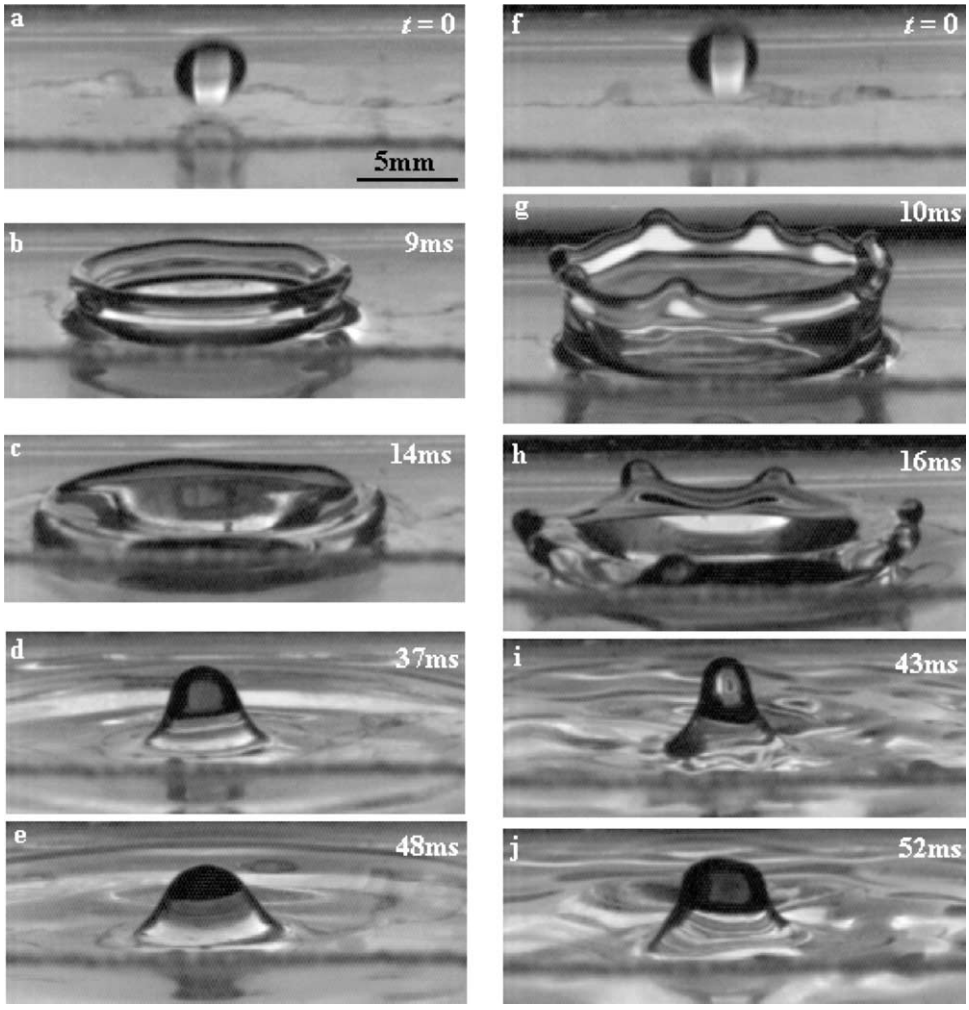

Fig. 12. Images of the impact of a water drop of diameter $D_0 = 3.59$ mm on a thin film of 17.5 mM CTAB/NaSal with dimensionless thickness $\delta = 0.5$. The images on the left are for a droplet impact velocity of $U = 1.9$ m/s and the images on the right are for $U = 3.2$ m/s.

observed to grow monotonically with increasing drop impact velocity even as the Worthington jet height reached a plateau.

The maximum Worthington jet height of the CTAB solutions before the onset of non-monotonic behavior is in all cases larger than that of water for the same drop impact velocity. This is markedly different from the results of Cheny and Walters [30] who found that the height of the Worthington jet decreased with increasing fluid elasticity of deep reservoirs of low concentration polymer solutions with constant viscosity, a Boger fluid. Cheny and Walters [30] hypothesized that the reduction in the Worthington jet height was a result of the large extensional viscosity of the polymer solutions. This hypothesis is consistent with their experiments as Worthington jets were produced with very large aspect ratios and therefore significant strain hardening could have been achieved. However, as described above, extensional rheology alone cannot be used to satisfactorily explain the experimental results in Figs. 10 and 11.

A series of experiments were performed to determine the importance of the dynamic surface tension on the dynamics of the Worthington jet. The equilibrium surface tension for these wormlike micelle solutions was found by Cooper-White et al. [27] to be $\sigma = 0.036$ N/m. However, because of the relatively short timescales associated with the droplet impact experiments, as new surface is created, the dynamic surface tension starts at the surface tension of water for about 20 ms before CTAB molecules begin diffusing from the bulk to populate the new surface. The surface tension will then begin to decay, eventually approaching an equilibrium value after about 1000 ms [27]. If the short time value of the surface tension is used to convert the impact velocity in Fig. 11 into a Weber number, then the Worthington jet height of the CTAB/NaSal solutions will be larger than that of water for all Weber numbers. However, if the equilibrium value of the surface tension is used, then as expected from the results of Cheny and Walters [30], the Worthington jet heights for the surfactant solutions will be smaller than water for all Weber numbers. To explicitly study the role of dynamic surface tension, a thin film of a 1 mM CTAB/NaSal solution was impacted with water droplets. The dynamic surface tension of the 1 mM CTAB/NaSal solution is identical to that of the more concentrated surfactant solutions [27] and because the concentration is so low, the fluid is not elastic and the viscosity is constant and roughly equal to that of water. Within experimental error, the observed impact dynamics of these experiments were identical to impact dynamics on a thin film of water. Thus, it appears that the short-time limit of the surface tension is the correct value to choose for these fast experiments. Additionally, these experiments suggest that the dynamic surface tension of the wormlike micelle solutions is most likely not the primary cause of the increase in Worthington jet height of the surfactant solutions over that of water or the odd behavior of the Worthington jet height as a function of Weber number observed in Fig. 11.

It is our hypothesis that the complex behavior of the Worthington jet height of the viscoelastic surfactant solutions is a direct result of the elastic effects generated within the thin film upon droplet impact. After impact, as the thin film spreads and the crown grows, the fluid experiences a very strong inhomogeneous biaxial extensional flow. The strength of the biaxial extensional flow can be estimated from the rim velocity of the crown, U_c, divided by the thickness of the thin film, t_f [45]

$$\dot{\varepsilon}_c(t) = \frac{U_c}{t_f} = \frac{1}{t_f}\frac{dR_c(t)}{dt}, \tag{10}$$

where R_c is the radius of the crown as a function of time. By measuring the crown radius as a function of time and then fitting the profile to a third order polynomial, estimates of the extension rates during crown growth of up to $\dot{\varepsilon}_c \approx 2000\,s^{-1}$ and accumulated strains of up to $\varepsilon_c \approx 3$ were calculated from Eqs. (10) and (9), respectively. The result of the elasticity of the thin film at low Weber numbers is to store some of the energy of the droplet impact as the crown grows and to return that energy to the crown as it recedes, thereby increasing the velocity of the receding crown and the height of the Worthington jet. As the impact velocity of the droplet is increased, the extensional and shear stresses within the thin film increase causing the wormlike micelles to align with the flow and stretch. At this point, the stress exerted on an individual micelle can be significant. Unlike an entangled polymer melt, which relieves stress through reptation or convected constraint release, micelles can break and then reform a short time later under Brownian fluctuations. Whereas a covalently bonded polymer chain can require energies on the order of 100s of k_BT to result in the scission of the macromolecule [46], the scission energy of a wormlike micelle is expected to only require 'a few' k_BT [47]. Here, k_B is the Boltzmann constant and T is the temperature. This perpetual break-up and reformation can lead to a broad and dynamic distribution of micelle lengths which can change under an imposed shear or extensional flow [9] and which can result in a wealth of complex phenomenon.

In some viscometric shear flows, wormlike micelle solutions have been found to exhibit the formation of banded structures or 'slip layers' of different surfactant morphologies having dramatically different rheological properties [48–54]. As seen in Fig. 5, as the imposed shear rate is increased, a critical shear rate is reached for each of the wormlike micelle solutions tested above which the shear stress approaches a constant, $\tau \approx$ constant, and the viscosity decays with a slope of $\eta \propto \dot{\gamma}^{-1}$. This behavior is synonymous with onset of shear banding. Through direct NMR measurements of the flow field within a cone-and-plate rheometer, Britton and Callahan [55] showed that as the shear rate was increased above this critical shear rate, the percentage of the flow occupied by these shear bands increased [55,56]. The plateau observed in the shear stress might therefore represent the maximum shear stress that can be supported by the wormlike micelles before they are broken into smaller, less elastic wormlike micelles, or inelastic spherical micelles.

At the shear rates experienced by the fluid beneath the impacting drops and for the extension rates imposed on the fluid as the crown expands, a cleavage of the wormlike micelles into shorter wormlike micelles or even spherical micelles is highly probable. The scission of the micelles is a dissipative phenomenon as energy must be supplied to create two additional endcaps every time a micelle is ruptured [6]. Thus, the plateau in the Worthington jet height can be explained in terms of this dissipative process. As the impact velocity and therefore the kinetic energy of the impacting droplet are increased, a critical stress is reached in the fluid above which the micelles begin to rupture. As the impact velocity is further increased, additional energy is dissipated as scission occurs in progressively more micelles. These arguments are consistent with the observations in Figs. 10 and 11, in which the critical Weber number for the onset of the non-monotonic behavior of the Worthington jet height is observed to increase with increasing micelle concentration and increasing film thickness. At larger surfactant concentrations, there are more wormlike micelles to carry the imposed load upon impact and therefore the stress experienced by each micelle is reduced. Additionally, as the film thickness is increased the extension rate experienced by the fluid during crown growth Eq. (10) as well as the Deborah number of impact Eq. (6) are decreased, reducing the extensional stresses developed in the thin film and forestalling the onset of micelle scission. As described in Section 2, the characteristic time for the break-up-recombination of these wormlike micelles, λ_{break}, is several hundred milliseconds. As seen from Fig. 12, the typical duration of an impact event is on the order of $t_{impact} \approx 40$–50 ms and thus we do not expect significant structural recovery over the course of these experiments. The applicability of λ_{break} to the reformation of wormlike micelles has been shown for small amplitude pressure-jump and temperature-jump experiments [35], however, its applicability to our experiments and others with large stress jumps and presumably significant microstructural disruption is less certain. In the absence of a more controlled experiment, the impact of multiple droplets on a thin film of wormlike micelle solutions might be an interesting way to probe recovery time of the micelle microstructure.

4. Conclusions

The impact dynamics of drops on thin films of viscoelastic wormlike micelle solutions was experimentally studied using a high-speed digital video camera. The experiments were performed using a series of wormlike micelle solutions composed of CTAB and NaSal dissolved in deionized water at concentrations between 10 mM and 25 mM. The composition and thickness of the thin film were modified to investigate the effect of fluid rheology on the evolution of crown growth, the formation of satellite droplets and the formation of the Worthington jet. In addition, the size and velocity of the impacting drop was varied to study the relative importance of Weber, Ohnesorge, and Deborah numbers on the impact dynamics.

The addition of elasticity to the thin film fluid was found to suppress the crown growth and the formation of satellite drops with the largest effects observed at small film thicknesses. A new form of the splashing threshold was postulated which accounts for the effects of viscoelasticity, $K_{L,VE} = Oh^{-0.37}\, We\, De^{-1}$, which successfully eliminated the effects of drop size and collapsed the satellite droplet data onto a single master curve at large dimensionless film thicknesses. A previously unobserved plateau was found in the growth of the maximum height of the Worthington jet with increasing impact velocity. The complex behavior of the Worthington jet growth is believed to be the result of a dissipative mechanism stemming from the scission of wormlike micelles under the strong extensional flow conditions.

Understanding the impact dynamics of droplets on thin films of viscoelastic wormlike micelle solutions is important to applications ranging from inkjet printing to the agrochemical spraying to spray coating.

Acknowledgements

The authors would like to thank the referees for the helpful comments and suggestions, Professor Menon of the University of Massachusetts for the use of his high speed video camera and 3M Non-Tenured Faculty Award for partial support of this research.

References

[1] M.E. Cates, Reptation of living polymers: dynamics of entangled polymers in the presence of reversible chain-scission reactions, Macromolecules 20 (1987) 2289–2296.
[2] H. Rehage, H. Hoffmann, Viscoelastic surfactant solutions: model systems for rheological research, Mol. Phys. 74 (1991) 933–973.
[3] T. Shikata, S.J. Dahman, D.S. Pearson, Rheo-optic behavior of wormlike micelles, Langmuir 10 (1994) 3470–3476.
[4] J.P. Rothstein, Transient extensional rheology of wormlike micelle solutions, J. Rheol. 47 (2003) 1227–1247.
[5] J.W. van Egmond, Shear-thickening in suspensions, associating polymers, worm-like micelles and polymer solutions, Curr. Opin. Colloid Interface Sci. 3 (1998) 385–390.
[6] J.N. Israelachvili, Intermolecular and Surface Forces: With Applications to Colloidal and Biological Systems, Academic Press, London, 1985.
[7] H. Rehage, H. Hoffmann, Rheological properties of viscoelastic surfactant systems, J. Phys. Chem. 92 (1988) 4712–4719.
[8] R.G. Larson, The Structure and Rheology of Complex Fluids, Oxford University Press, New York, 1999.
[9] M.E. Cates, M.S. Turner, Flow-induced gelation of rodlike micelles, Europhys. Lett. 11 (1990) 681–686.
[10] G.H. McKinley, T. Sridhar, Filament stretching rheometry, Annu. Rev. Fluid Mech. 34 (2002) 375–415.
[11] S. Chen, J.P. Rothstein, Flow of a wormlike micelle solution past a falling sphere, J. Non-Newtonian Fluid Mech. 116 (2004) 205–234.
[12] H.A. Stone, Dynamics of drop deformation and breakup in viscoelastic fluids, Annu. Rev. Fluid Mech. 26 (1994) 65–102.

[13] S.L. Anna, G.H. McKinley, Elasto-capillary thinning and breakup of model elastic liquids, J. Rheol. 45 (2001) 115–138.
[14] M. Renardy, A numerical study of the asymptotic evolution and breakup of Newtonian and viscoelastic jets, J. Non-Newtonian Fluid Mech. 59 (1995) 267–282.
[15] R.K. Prud'homme, G.G. Warr, Elongational flow of solutions of rodlike micelles, Langmuir 10 (1994) 3419–3426.
[16] L.B. Smolka, A. Belmonte, Drop pinch-off and filament dynamics of wormlike micellar fluids, J. Non-Newtonian Fluid Mech. 115 (2003) 1–25.
[17] C. Chen, G.G. Warr, Light scattering from wormlike micelles in an elongational flow, Langmuir 13 (1997) 1374–1376.
[18] A. Jayaraman, A. Belmonte, Oscillations of a solid sphere falling through a wormlike micelle solution, Phys. Rev. E 67 (2003) 065301.
[19] A. Belmonte, Self-oscillations of a cusped bubble rising through a micellar solution, Rheol. Acta 39 (2000) 554–559.
[20] N.Z. Handzy, A. Belmonte, Oscillatory rise of bubbles in wormlike micellar fluids with different microstructures, Phys. Rev. Lett. 92 (2004) 124501–124504.
[21] B.L. Sheller, D.W. Bousfield, Newtonian drop impact with a solid surface, AIChE J. 41 (1995) 1357–1367.
[22] M. Rein, The transitional regime between coalescing and splashing drops, J. Fluid Mech. 306 (1996) 145–165.
[23] C.D. Stow, M.G. Hadfield, An experimental investigation of fluid flow resulting from the impact of a water drop with an unyielding dry surface, Proc. R. Soc. Lond. A 373 (1981) 419–441.
[24] G.E. Cossali, A. Coghe, M. Marengo, The impact of a single drop on a wetted solid surface, Exp. Fluids 22 (1997) 463–472.
[25] A.-B. Wang, C.-C. Chen, Splashing impact of a single drop onto very thin liquid films, Phys. Fluids 12 (2000) 2155–2158.
[26] R. Crooks, D.V. Boger, Influence of fluid elasticity on drop impacting on dry surfaces, J. Rheol. 44 (2000) 973–996.
[27] J.J. Cooper-White, R.C. Crooks, D.V. Boger, A drop impact study of worm-like viscoelastic surfactant solutions, Colloids Surf. A: Physicochem. Eng. Aspects 210 (2002) 105–123.
[28] J.J. Cooper-White, R.C. Crooks, K. Chockalingam, D.V. Boger, Dynamics of polymer-surfactant complexes: elongational properties and drop impact behavior, Ind. Eng. Chem. Res. 41 (2002) 6443–6459.
[29] R. Crooks, J.J. Cooper-White, D.V. Boger, The role of dynamic surface tension and elasticity on the dynamics of drop impact, Chem. Eng. Sci. 56 (2001) 5575–5592.
[30] J.M. Cheny, K. Walters, Extravagant viscoelastic effects in the Worthington jet experiment, J. Non-Newtonian Fluid Mech. 67 (1996) 125–135.
[31] J.M. Cheny, K. Walters, Rheological influence on the splashing experiment, J. Non-Newtonian Fluid Mech. 86 (1999) 185–204.
[32] K. Range, F. Feuillebois, Influence of surface roughness on liquid drop impacet, J. Colloid Interface Sci. 203 (1998) 16–30.
[33] P. Fischer, H. Rehage, Rheological master curves of viscoelastic surfactant solutions by varying the solvent viscosity and temperature, Langmuir 13 (1997) 7012–7020.
[34] J.-F. Berret, J. Appell, G. Porte, Linear rheology of entangled Wormlike micelles, Langmuir 9 (1993) 2851–2854.
[35] A. Khatory, F. Lequeux, F. Kern, S.J. Candau, Linear and nonlinear viscoelasticity of semidilute solutions of wormlike micelles at high salt concentration, Langmuir 9 (1993) 1456–1464.
[36] M.S. Turner, M.E. Cates, Linear viscoelasticity of living polymers: a quantitative probe of chemical relaxation times, Langmuir 7 (1991) 1590–1594.
[37] R. Granek, M.E. Cates, Stress relaxation in living polymers: results from a Poisson renewal model, J. Chem. Phys. 96 (1992) 4758–4767.
[38] R.B. Bird, R.C. Armstrong, O. Hassager, Dynamics of Polymeric Liquids: Fluid Mechanics, vol. 1, John Wiley & Sons, New York, 1987.
[39] J.P. Rothstein, G.H. McKinley, Inhomogeneous transient uniaxial extensional rheometry, J. Rheol. 46 (2002) 1419–1443.
[40] J.P. Rothstein, G.H. McKinley, A comparison of the stress and birefringence growth of dilute, semi-dilute and concentrated polymer solutions in uniaxial extensional flows, J. Non-Newtonian Fluid Mech. 108 (2002) 275–290.
[41] L.E. Wedgewood, D.N. Ostrov, R.B. Bird, A finite extensible bead-spring chain model for dilute polymer-solutions, J. Non-Newtonian Fluid Mech. 40 (1991) 119–139.
[42] L. Rayleigh, On the capillary phenomena of jets, Proc. R. Soc. Lond. 29 (1879) 71–97.
[43] J. Eggers, Nonlinear dynamics and breakup of free-surface flows, Rev. Mod. Phys. 69 (1997) 865–929.
[44] A.L. Yarin, Free Liquid Jets and Films: Hydrodynamics and Rheology, Wiley, New York, 1993.
[45] V. Bergeron, D. Bonn, J.Y. Martin, L. Vovelle, Controlling droplet deposition with polymer additives, Nature 405 (2000) 772–775.
[46] J.A. Odell, A. Keller, Y. Rabin, Flow-induced scission of isolated macromolecules, J. Chem. Phys. 88 (1988) 4022–4028.
[47] M.S. Turner, M.E. Cates, Flow-induced phase transitions in rod-like micelles, J. Phys. Condens. Matter. 4 (1992) 3719–3741.
[48] Y. Hu, P. Boltenhagen, E. Matthys, D.J. Pine, Shear thickening in low-concentration solutions of wormlike micelles. II. Slip, fracture, and stability of the shear-induced phase, J. Rheol. 42 (1998) 1208–1226.
[49] R.G. Larson, Flow-induced mixing, demixing, and phase-transitions in polymeric fluids, Rheol. Acta 31 (1992) 497–520.
[50] R.W. Mair, P.T. Calaghan, Observation of shear banding in wormlike micelles by NMR velocity imaging, Europhys. Lett. 36 (1996) 719–724.
[51] J.-F. Berret, D.C. Roux, P. Lindner, Structure and rheology of concentrated wormlike micelles at the shear-induced isotropic-nematic transition, Eur. Phys. J. B 5 (1998) 67–77.
[52] I.A. Kadoma, J.W. van Egmond, Flow-induced nematic string phase in semidilute wormlike micelle solutions, Phys. Rev. Lett. 80 (1998) 5679–5682.
[53] C.H. Liu, D.J. Pine, Shear-induced gelation and fracture in micellar solutions, Phys. Rev. Lett. 77 (1996) 2121–2124.
[54] E.K. Wheeler, P. Fischer, G.G. Fuller, Time-periodic flow induced structures and instabilities in a viscoelastic surfactant solution, J. Non-Newtonian Fluid Mech. 75 (1998) 193–208.
[55] M.M. Britton, P.T. Callaghan, Nuclear magnetic resonance visualization of anomalous flow in cone-and-plate rheometry, J. Rheol. 41 (1997) 1365–1386.
[56] Y. Hu, P. Boltenhagen, D.J. Pine, Shear thickening in low-concentration solutions of wormlike micelles. I. Direct visualization of transient behavior and phase transitions, J. Rheol. 42 (1998) 1185–1208.